ACS OMEGA

http://pubs.acs.org/journal/acsodf

Article

Green Fabrication of Bioactive Silver Nanoparticles Using *Mentha pulegium* Extract under Alkaline: An Enhanced Anticancer Activity

Yinghui Wang and Simin Wei*

Cite This: *ACS Omega* 2022, 7, 1494−1504

Read Online

ACCESS | Metrics & More | Article Recommendations | Supporting Information

ABSTRACT: Fabrication of silver nanoparticles (AgNPs) using Chinese herbal medicine is popular as the bioactive components included in them would generate potential synergistic effect with the metal nanoparticles. The leaf of *Mentha pulegium*, whose extract contains a range of phytochemicals and exhibits a wide spectrum of bioactivities, is used as Chinese herbal medicine after drying naturally. Thus, the green synthesis of AgNPs using *Mentha pulegium* has aroused interests from analysts. However, the biosynthesis of AgNPs under alkaline conditions and the biological activities remain elusive, where alkaline conditions may influence the physicochemical properties and the biological activities of biosynthesized AgNPs. In this study, we were stimulated to fabricate bioactive AgNPs using *Mentha pulegium* extract under alkaline conditions, accompanied by a systematic evaluation on the effect of biosynthesis parameters on the formation, average size, and polydispersity of AgNPs. Our results showed that alkaline conditions could accelerate the formation of AgNPs with a small average size but at a disadvantage to the polydispersity. Additionally, the as-prepared AgNPs had a hexagonal structure and spherical shape with an average size of 15.7 ± 0.1 nm, existing in the monodispersed form and revealing a high degree of stability. The AgNPs exhibited potent antioxidant and significant inhibitory activity for both bacterial and cancer cell lines. The MIC values of AgNPs for *Staphylococcus aureus* and *Escherichia coli* were both 50.0 $\mu g \cdot mL^{-1}$, and the IC_{50} values for HCT116, HepG2, and HeLa cells were 9.0, 14.5, and 31.5 $\mu g \cdot mL^{-1}$, respectively. The AgNPs biosynthesized using *M. pulegium* under alkaline conditions, which had a smaller size and more surface loads, are entirely different with those synthesized under acidic conditions, and the anticancer activity increased significantly. The internalization of AgNPs inside these five cells displayed a variant trend with variable AgNPs concentrations, suggesting the different mechanism of cell death. For two pathogens, HCT116 and HepG2 cancer cell lines, both cell wall and intracellular damage may be responsible for the cell death. However, for Hela cell line the cell death may be rooted in oxidative stress or intracellular penetration. These results confirmed that the AgNPs biosynthesized from *M. pulegium* extract under alkaline conditions would act as better anticancer agents in biomedicine.

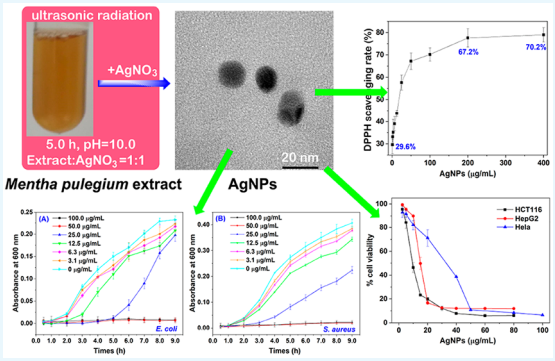

1. INTRODUCTION

Due to their high biocompatibility, lower toxicity, and broad spectrum of bioactive activities like antimicrobial and anticancer activities, silver nanoparticles (AgNPs) have been widely applied as the active ingredient delivery vehicles, diagnosis, and therapy.[1−14] Thus, the synthesis of AgNPs is a subject matter with great scientific interest. Although various physicochemical methods such as autoclaving, γ-ray radiation, and the use electrochemical techniques and chemical reduction can produce high yield of AgNPs, they consume lots of energy and may cause adverse biological effects because of the introduction of toxic reducing and capping agents.[15−21] Therefore, bioresources like plant extracts are more popular in the synthesis of AgNPs for biomedical purposes.[22−26] Biological agents are not only biocompatible, degradable, environment friendly, and cost-effective but also provide the stable coating layers to prevent the aggregation of particles and afford a reduction force to metal precursors.[27] Many studies have shown that when these biological agents displayed biological activities, a synergistic effect between the metal nanoparticles and these bioactive molecules would be obtained.[22,27] Thus, traditional Chinese medicines have attracted considerable attention from analysts due to medicinal components in them.[28−34] To date, numerous Chinese herbal medicines such as *Sea buckthorn*,[30,35] *Zizyphus mauritiana*,[36] *Nelumbo nucifera*,[37,38] and *Cornus officinalis*[31,33,39,40] have been employed for the synthesis of bioactive AgNPs.

Mentha pulegium, which belongs to the family *Lamiaceae* and is native to humid regions like China and Iran, is a traditional medicine to treat colds, sinusitis, cholera, food poisoning,

Received: November 7, 2021
Accepted: December 17, 2021
Published: December 30, 2021

Scheme 1. Schematic of the Green Fabrication of AgNPs using *Mentha pulegium* Leaf Extract As the Bioreductant

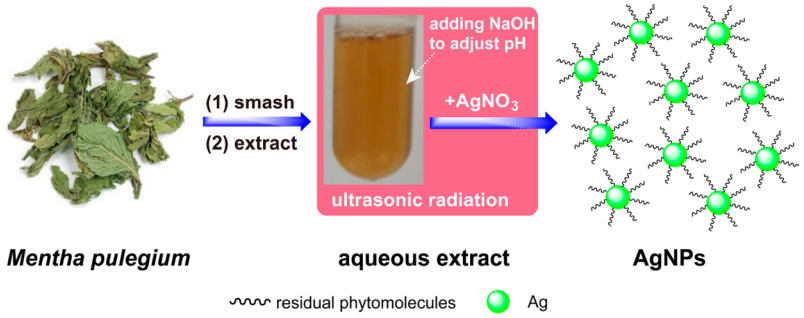

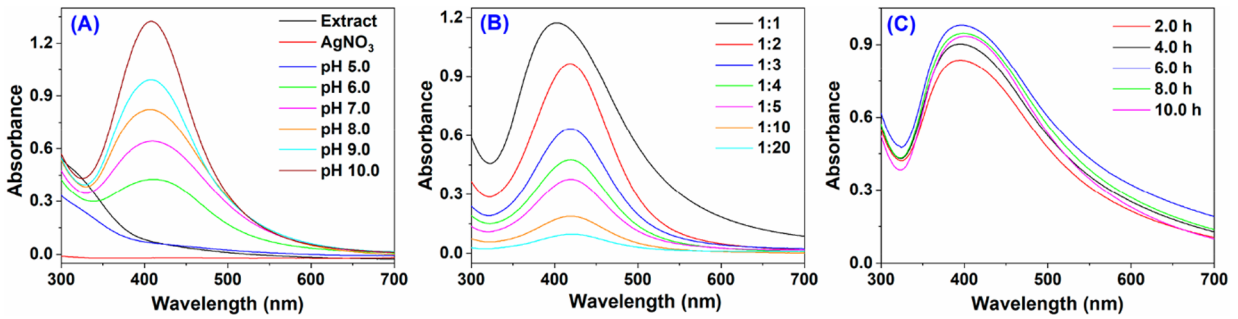

Figure 1. UV−vis spectra of the mixture after the reaction between the *Mentha pulegium* leaf extract and $AgNO_3$ at different (A) pH levels, (B) material ratios, and (C) incubation times.

bronchitis, and tuberculosis.[41] Studies have shown that *Mentha pulegium* contains a range of bioactive chemicals like essential oils, isomenthone, menthoacetate, peppermint isoflavourin, and rosmarinic acid, which exhibit a wide spectrum of antioxidant, antimicrobial, and anticancer activities.[41−44] It is possible to fabricate AgNPs with superior bioactivities using *Mentha pulegium*. On this basis, Abdol-Khalegh Bordbar[45] and Hadi Faranak[46] have successfully synthesized AgNPs using *Mentha pulegium* leaf extract, which revealed significant inhibition of bacterial strains as well as the cancer cell lines but no cytotoxicity for human peripheral blood mononuclear cells (PBMCs). We noticed that both Abdol-Khalegh Bordbar and Hadi Faranak used the primary extract of the *Mentha pulegium* leaf, which is an acidic solution. It has been indicated that an alkaline solution may accelerate the formation of AgNPs with a small size and mediate the surface charge, which are directly related to the biological activities.[22,31] The AgNPs with different sizes, shapes, and ζ-potentials would exhibit different antimicrobial and anticancer activities due to displaying various degrees of membrane permeability and electrostatic adhesion between AgNPs and the cell membrane.[22] What the physicochemical properties and biological activities of biosynthesized AgNPs under alkaline conditions are is a fascinating subject. Additionally, it is clear that evaluating the effects of biosynthesis parameters on the physicochemical properties of nanoparticles will play an important role in regulating their biological activities. However, these studies remain elusive to a large extent in past investigations. Obviously, further study on the green synthesis of AgNPs using *Mentha pulegium* should be proceeded.

Herein, we present the biosynthesis of AgNPs using *Mentha pulegium* extract under alkaline conditions at ambient temperature (Scheme 1), where a systematically investigation about the effects of biosynthesis parameters on the reducing reaction and physicochemical properties of AgNPs was performed. Additionally, the crystalline nature, size, shape, surface properties, stability, and biological activities, including antioxidant, antimicrobial, and anticancer activities, of biosynthesized AgNPs were assessed thoroughly and were entirely different from those of AgNPs synthesized under acidic conditions. The mechanism of cell death was also preliminarily speculated by investigating the internalization of as-prepared AgNPs. These results reveal that the reducing reaction and physicochemical properties of as-prepared AgNPs are sensitive to the biosynthesis parameters, and the AgNPs biosynthesized using *Mentha pulegium* at alkaline conditions could also act as a promising candidates for antioxidant, antimicrobial, and anticancer drugs.

2. RESULTS AND DISCUSSION

According to previous studies,[47−49] biosynthesis parameters like the pH of the extract, the material proportion, and the incubation time could influence the formation and physicochemical properties of nanoparticles, playing pivotal roles in controlling the chemical, physical, electronic, and optical properties of these nanoscopic materials. Thus, the effects of biosynthesis parameters on the formation, average size, and polydispersity of AgNPs were evaluated systematically.

2.1. Effect of Biosynthesis Parameters on the Formation of AgNPs. The primary extract of *Mentha pulegium* leaf (pH 5.0) was initially used to prepare AgNPs by mixing it (5.0 mL) with 10 mM $AgNO_3$ (5.0 mL) under ultrasonic radiation at ambient temperature. After 1.0 h of incubation, however, there were not any obvious changes in the color of the mixed solution (Figure S1). As shown in previous studies,[50,51] the formation of AgNPs would turn the color of mixed solution to dark brown. This result indicates that the primary extract of *Mentha pulegium* is helpless for

https://doi.org/10.1021/acsomega.1c06267
ACS Omega 2022, 7, 1494−1504

reducing Ag^+ to Ag^0 within 1.0 h. This may originate from the slow formation rate, which results in very little AgNP generation. To further confirm this conclusion, UV−vis spectroscopy measurements were performed where AgNPs had a distinct absorption peak in 400−500 nm as the surface plasmon resonance (SPR). Figure 1A shows the UV−vis spectrum of the mixture after 1.0 h of incubation, where the absorbance of the *Mentha pulegium* leaf extract and $AgNO_3$ were negligible. The spectrum of mixture in the 400−500 nm range is almost similar to that of *Mentha pulegium* leaf extract alone, which essentially agrees with the observation in color by the naked eye.

According to a previous study,[52] adjusting the pH of a plant extract to alkalinity may accelerate AgNP formation. Thus, we then tried to performed the reaction at pH 6.0. The color of the mixed solution changed from yellow to brown after 1.0 h of incubation (Figure S1), suggesting the generation of AgNPs. The UV−vis spectrum for the *Mentha pulegium* leaf extract and $AgNO_3$ at pH 6.0 obtained after the 1.0 h reaction reveals a strong absorption band that peaks at 412 nm (Figure 1A). The spectrum characteristics essentially resembled those from previous studies about the SPR peak of AgNPs,[30,52] further confirming that AgNPs were successfully prepared. Subsequently, the pH of the *Mentha pulegium* leaf extract was successively increased. When the pH was increased to 10.0, the absorption band around 412 nm sharply increased, accompanyied with the slight shift of SPR peak to 407 nm (Figure 1A). The enhanced SPR band intensity should reflect the increased formation amount of AgNPs. The slight blue-shift of the SPR peak from 412 to 407 nm suggests that the formed AgNPs have different sizes (see below). This may originate from the increased bioavailabity of functional groups at high pH that favors the AgNP product, leading to a faster nucleation rate. This result is in accord with the perspective obtained from previous studies that biosynthesis of AgNPs is a pH-dependent reaction.[52]

Then, to assess the effect of the material proportion on the formation of AgNPs, the experiment was performed at pH 10.0, where the volumes of $AgNO_3$ (5.0 mL) and the mixed solution (10.0 mL) were kept constant. Figure 1B displays the UV−vis spectra of mixed solutions at different ratios after 4.0 h of incubation at ambient temperature. When the reaction was performed on the ratio 1:20 (*Mentha pulegium* leaf extract/$AgNO_3$), a weak band with a maximum absorbance around 422 nm was observed. Additionally, as the material proportion of *Mentha pulegium* leaf extract and $AgNO_3$ gradually increased to 1:1, the peak intensity also increased, accompanyed with the band shift to 403 nm. The increased peak intensity and band shift to blue indicate the increased production yield and different sizes of AgNPs, respectively. It seems that more *Mentha pulegium* leaf extract would be benefit the generation of AgNPs. However, it is difficult for us to obtain an extract with larger concentrations, since the extract is thick enough.

Figure 1C shows the absorption spectra of AgNPs after incubating 5.0 mL of *Mentha pulegium* leaf extract (pH 10.0) and 5.0 mL of $AgNO_3$ with different times. The featured SPR band of AgNPs was clearly observed after 2.0 h of ultrasonic radiation at ambient temperature. Additionally, the absorption intensity enhanced steadily with the passage of time and reached a maximum after 6.0 h, indicating an increased amount of AgNPs and the fully completed reduction reaction within 6.0 h. The UV−vis spectra display a negligible band shift within 6.0 h, but with an obvious band shift after 6.0 h of incubation. The band shift may also result from different sizes of biosynthesized AgNPs. It is clear that biosynthesis of AgNPs with 5.0 mL of 10 mM $AgNO_3$ and 5.0 mL of *Mentha pulegium* leaf extract at pH 10.0 would have the maximum efficiency.

2.2. Effect of Biosynthesis Parameters on the Average Size of AgNPs. Then, the effects of biosynthesis parameters on the average size of biosynthesized AgNPs were systematically assessed, which could further confirm the origin of spectral evolution. The average size of biosynthesized AgNPs was measured by the dynamic light scattering (DLS) method, and the results are shown in Figure 2 and Table S1. It

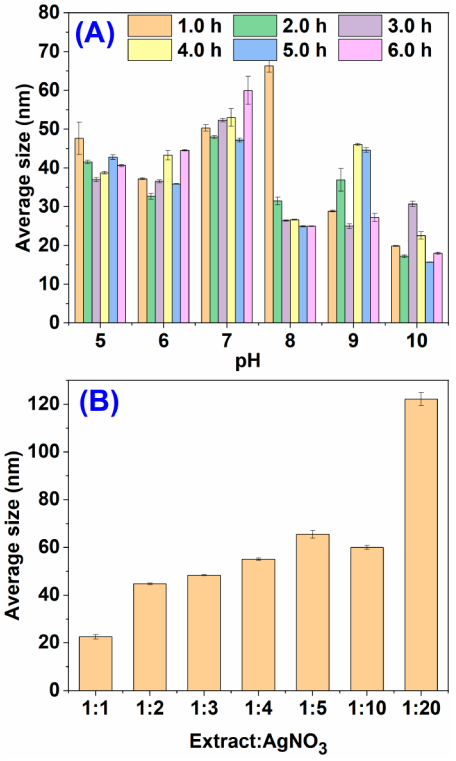

Figure 2. Average size of AgNPs biosynthesized using *Mentha pulegium* leaf extract at different (A) pH levels and incubation times and (B) material ratios.

is clear that when the material ratio of *Mentha pulegium* leaf extract and $AgNO_3$ is 1:1 the average size of biosynthesized AgNPs at an alkaline pH is smaller than that at an acidic pH (Figure 2A), which is basically in accordance with Sathishkumar[53] and Heydari's[54] view that an alkaline solution could accelerate the formation of AgNPs with a small size. This distribution of average size could also illustrate the evolution of our UV−vis spectrum shown previously. However, there are still some difference between our results and those from previous studies. It was shown that at pH 7.0 the biosynthesized AgNPs have a larger average size at almost all the incubation times. The biggest (66.3 ± 1.7 nm) and smallest (15.7 ± 0.1 nm) average sizes of AgNPs could be obtained at pH 8.0 after 1.0 h of incubation and pH 10.0 after 5.0 h of incubation, respectively. The influence of the material ratio on the average size of AgNPs was also evaluated at pH 10.0 after incubation for 4.0 h. As shown in Figure 2B and Table S2, with the addition of *Mentha pulegium* leaf extract into the mixture, the average size of AgNPs gradually decreased from 122.2 ± 2.7 to 22.6 ± 0.9 nm. This may originate from

https://doi.org/10.1021/acsomega.1c06267
ACS Omega 2022, 7, 1494−1504

the faster nucleation rate, since more reducing substances are included in the reaction mixture.

2.3. Effect of Biosynthesis Parameters on the Polydispersity of AgNPs. The polydispersity index (PDI), which is an important parameter for nanoparticles and could affect the characteristics of nanoparticles, was also assessed thoroughly. Studies have reported that if the sample has a PDI value lower than 0.3, it would exist in the monodisperse form.[55] Figure 3 and Table S3 display the PDIs of biosynthesized AgNPs under different biosynthesis parameters. As shown in Figure 3A, when the material ratio of *Mentha pulegium* leaf extract and $AgNO_3$ is 1:1, the biosynthesized AgNPs at an acidic pH have smaller PDI values compared with those synthesized at an alkaline solution on the whole. The smallest and largest PDI values were obtained when the experiments were performed at pH 5.0 after 2.0 h of incubation and at pH 10.0 after 6.0 h of incubation, respectively. The smallest PDI value is 0.23 ± 0.01, indicating a superior monodispersity. The material ratio also has significant influence on the PDI of biosynthesized AgNPs (Figure 3B and Table S4). At pH 10.0 after incubation for 4.0 h, the best monodispersed AgNPs were obtained with the material ratio of 1:3, where the PDI value was 0.21 ± 0.01.

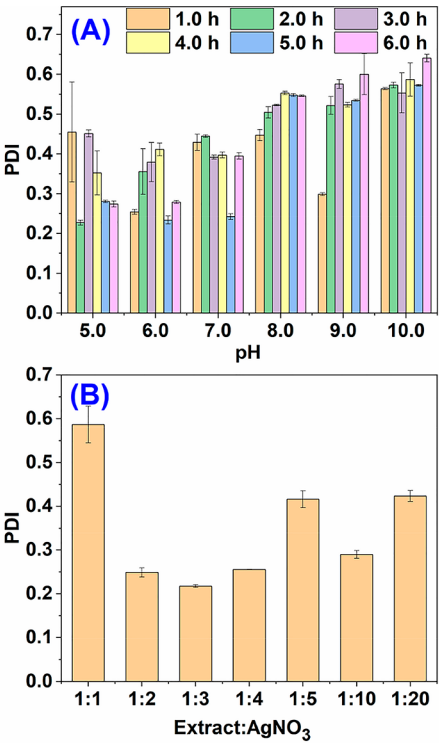

Figure 3. Polydispersity index (PDI) of AgNPs biosynthesized using *Mentha pulegium* leaf extract at different (A) pH levels and incubation times and (B) material ratios.

To obtain more products with a small size for further characterization and biological activity studies, we prepared AgNPs using 5.0 mL of 10 mM $AgNO_3$ and 5.0 mL of *Mentha pulegium* leaf extract (pH 10.0) after 5.0 h of incubation.

2.4. Characterization of Biosynthesized AgNPs. The experiments of energy dispersive X-ray spectroscopy (EDX), TEM, HRTEM, selected area electron diffraction (SAED), and DLS were performed to characterize the proper synthesis, crystalline nature, size, shape, and surface properties of biosynthesized AgNPs. The EDX spectrum (Figure 4A) displays a strong absorption peak around 3 keV, which relates to the presence of elemental silver in the nanoparticles. Another two strong signals in the EDX spectroscum are for carbon and copper, which should partially originate from the carbon-coated copper grid used in the TEM and EDX analysis. The EDX result further confirms the generation of AgNPs after a period of incubation of *Mentha pulegium* leaf extract and Ag^+.

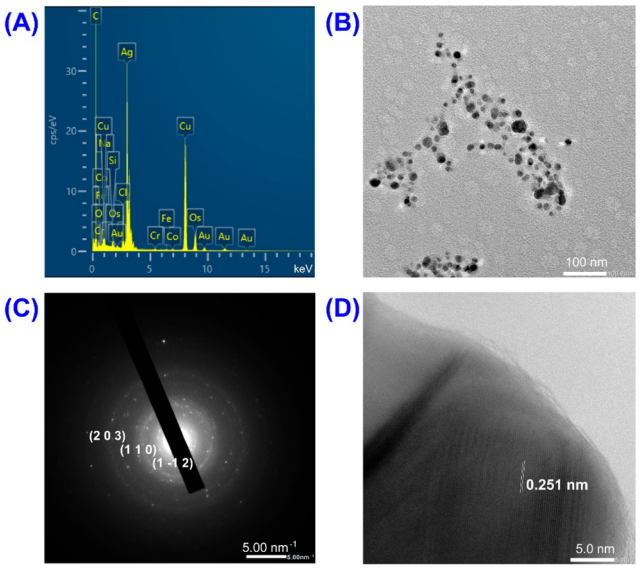

Figure 4. (A) EDX spectrum, (B) TEM image, (C) SAED image, and (D) HRTEM image.

Figure 4B shows the TEM image for biosynthesized AgNPs, which are mainly spherical in shape and have good dispersion and scattering in nature for a large proportion of the particles. It is obviously that the biosynthesized AgNPs have diameters roughly in the range of 10−20 nm basically in accordance with DLS results (15.7 ± 0.1 nm), which are smaller than those synthesized using *Mentha pulegium* extract under acidic condition.[45,46]

The SAED pattern and HRTEM spectrum as shown in Figure 4C and D, respectively, were used to prove the crystalline nature of as-prepared AgNPs. Three circular rings with *d*-values of 2.255, 1.420, and 1.159 Å in the SAED pattern (Figure 4C) were observed, which corresponded to the characteristic reflections of hexagonal crystalline silver for (1 $\bar{1}$ 2), (1 1 0), and (2 0 3) facets. This indicates the formation of hexagonal crystalline AgNPs. The lattice fringe was also measured to illustrate the crystalline nature of biosynthesized AgNPs. The measured *d*-value was 2.510 Å (Figure 4D), which was assigned to (0 0 4) facets of hexagonal crystalline AgNPs, further confirming the result about the crystalline nature obtained from the SAED pattern. The crystalline nature of biosynthesized AgNPs herein is different from that biosynthesized by Abdol-Khalegh Bordbar[45] and Hadi Faranak,[46] which may originate from the different nanocomposite.[56]

Lastly, the ζ-potential was used to assess the surface state and the long-term stability of biosynthesized AgNPs. Previous studies reported that the nanoparticles with ζ-potentials between −25.0 and +25.0 mV would have interparticle attractions and eventually lead to the aggregation of nanoparticles.[54] In parallel, the nanoparticles with ζ-potentials outside of the interval would have superior stability. As shown

https://doi.org/10.1021/acsomega.1c06267
ACS Omega 2022, 7, 1494−1504

in Table S5, the ζ-potential of AgNPs biosynthesized by *Mentha pulegium* leaf extract at pH 10.0 (−24.0 mV) was close to boundary of −25.0 mV, indicating a high degree of stability. Practically, the average size of the biosynthesized AgNPs after 45 days (21.7 ± 0.5 nm) reveals only a slightly change. Here, the ζ-potential obtained at pH 10.0 is smaller than that obtained by Abdol-Khalegh Bordbar (−15.9 mV) using *Mentha pulegium*[45] and us at lower pH (Table S5). The negative ζ-potential also suggests the electronegative capping agents in the surface of AgNPs. These molecules may be flavonoids, terpenoids, polyphenols, and proteins contained in *Mentha pulegium* extract, which have been confirmed by previous FTIR studies from Abdol-Khalegh Bordbar[45] and Hadi Faranak.[46]

2.5. Antioxidant Activities of Biosynthesized AgNPs. Based on previous studies,[41,42] *Mentha pulegium* contained more than 25 species, such as a high content of essential oils. Several authors have documented the antioxidant activity of *Mentha pulegium* extracts and the essential oils originating from *Mentha pulegium*.[42] As AgNPs would be coating by the bioactive constituent involved in the *Mentha pulegium* leaf extract, the AgNPs biosynthesized using *Mentha pulegium* leaf extract are anticipated to exhibit powerful antioxidant activity. Thus, we performed the DPPH experiment to evaluate the antioxidant activity of biosynthesized AgNPs, where the DPPH method is considered as one of the quickest methods. DPPH is a stable free radical, and its color would change from purple to yellow when it accepted hydrogen and electrons from the donors. Different concentrations of biosynthesized AgNPs were added into DPPH solution for the purpose of scavenging free radicals. As shown in Figure 5, the as-prepared AgNPs

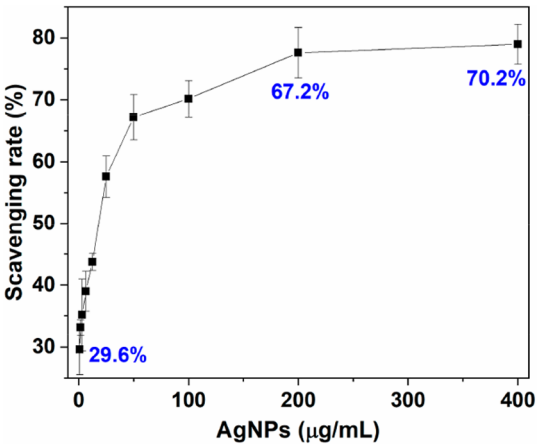

Figure 5. Free radical scavenging rate of biosynthesized AgNPs against DPPH.

reveal significant DPPH scavenging activity, which increased in a dose-dependent manner and had scavenging activities of 67.2% in 200.0 $\mu g \cdot mL^{-1}$ of AgNPs. However, when increasing the amount of AgNPs to 400.0 $\mu g \cdot mL^{-1}$, the scavenging activity slightly changed to 70.2%. The DPPH scavenging activity of AgNPs is comparable with those from previous reports by KUP[57] and Kivcak,[58] indicating that the AgNPs synthesized by using *Mentha pulegium* leaf extract could be used in treatment of many diseases caused by oxidative stress.

2.6. Antibacterial Activities of Biosynthesized AgNPs. The antibacterial activities of as-prepared AgNPs against both *Escherichia coli* (*E. coli*) and *Staphylococcus aureus* (*S. aureus*) were evaluated by measuring the absorbance of bacteria at 600 nm. Figure 6 displays the growth kinetics for these two

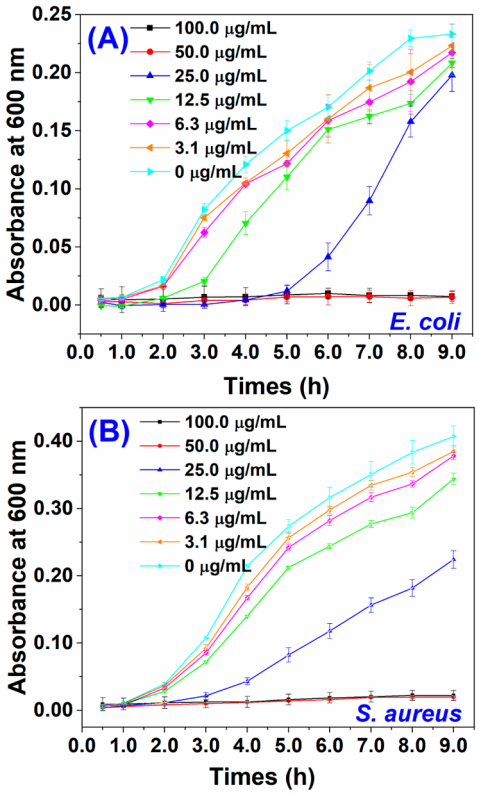

Figure 6. Antibacterial activity of biosynthesized AgNPs for (A) *E. coli* and (B) *S. aureus*.

pathogens after treatment with different doses of AgNPs, exhibiting a potential dose-dependent manner. It clearly reveals that even after treatment with 3.1 $\mu g \cdot mL^{-1}$ AgNPs, the growth of both pathogens would be inhibited. When incubating these two pathogens with 50.0 $\mu g \cdot mL^{-1}$ AgNPs, the growth of both *E. coli* and *S. aureus* was effectively inhibited within 9.0 h, indicating that the minimum inhibition concentrations (MIC) of as-prepared AgNPs were 50.0 $\mu g \cdot mL^{-1}$. The tests of zone inhibition, which were performed using the oxford cup method, also show significant inhibition for both bacterial strains against the nanomaterials (Figure S2). The MIC of AgNPs obtained herein is slightly different from those obtained by Abdol-Khalegh Bordbar (*E. coli* and *S. aureus*, 25 $\mu g \cdot mL^{-1}$)[45] and Hadi Faranak (*S. aureus*, 61.5 $\mu g \cdot mL^{-1}$; *E. coli*, 125 $\mu g \cdot mL^{-1}$)[46] using *Mentha pulegium* leaves. We speculated that might arise from different chemical constituents of the *Mentha pulegium* extract used in the biosynthesis of AgNPs, which have a significant effect on the affinity of AgNPs for phosphorus- and sulfur-containing compounds on the cell.[59]

2.7. Anticancer Activities of Biosynthesized AgNPs. The anticancer activities of the biosynthesized AgNPs against HCT116, HepG2, and HeLa were preliminarily assessed by exposing these three cancer cell lines to AgNPs at concentrations in the range of 0−100 $\mu g \cdot mL^{-1}$ for 24.0 h. MTT assays were performed to determine the cytotoxicity of AgNPs for these cancer cell lines. As shown in Figure 7, after treating these cancer cell lines with AgNPs, the cell viability decreased in a dose-dependent fashion. With increased doses of AgNPs, the cell viability of AgNP-treated cell lines

https://doi.org/10.1021/acsomega.1c06267
ACS Omega 2022, 7, 1494−1504

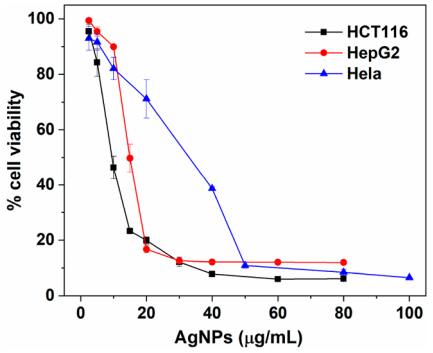

Figure 7. Inhibition effects of biosynthesized AgNPs on HCT116, HepG2, and Hela cell lines.

significantly decreased. In the cases of HCT116 and HepG2 cell lines, cell viabilities were significantly decreased to 19.9% and 16.7% at 20.0 $\mu g{\cdot}mL^{-1}$ AgNPs and to 6.1% and 11.9% at 80.0 $\mu g{\cdot}mL^{-1}$ AgNPs, respectively. On the other hand, for the Hela cell line, the cell viability was 10.9% at 50.0 $\mu g{\cdot}mL^{-1}$ AgNPs and 6.5% at 100.0 $\mu g{\cdot}mL^{-1}$ AgNPs. The IC_{50} values of AgNPs against HCT116, HepG2, and HeLa cancer cell lines were determined by fitting the curve of the cell viability using the GraphPad Prism 8.0 software package, and the values were 9.0, 14.5, and 31.5 $\mu g{\cdot}mL^{-1}$, respectively. The AgNPs synthesized by the *Mentha pulegium* extract herein displayed a higher anticancer activity than the AgNPs synthesized by Hadi Faranak using Iranian *Mentha pulegium* (~100 $\mu g{\cdot}mL^{-1}$ for Hela and MCF-7),[46] and other traditional medicines with an anticancer effect, such as *Iresine herbstii*[60] (51 $\mu g{\cdot}mL^{-1}$ for Hela) and *Cornus officinalis*[31] (20.68 and 69.72 $\mu g{\cdot}mL^{-1}$ for HCT116 and HepG2, respectively). Additionally, these values were also comparable to those of *Sea buckthorn*[30] (8.77, 14.59, and 27.98 $\mu g{\cdot}mL^{-1}$ for HCT116, HepG2, and HeLa, respectively), indicating that the AgNPs biosynthesized using *Mentha pulegium* extract could be acted as candidate for anticancer drugs.

2.8. Internalization of Biosynthesized AgNPs. To clearly elucidate the mode of action between the cell and the nanoparticles, three well-defined mechanisms have been proposed: (i) cell wall and membrane damage, (ii) intracellular penetration and damage, and (iii) oxidative stress.[27,61] Obviously, assessing the internalization of AgNPs into cells would benefit the understanding of the cell death mechanism. Previous studies are available that show granules in cytoplasm could scatter more light in the perpendicular direction (90°) of an incident laser (488 nm), defined as the side scattering channel (SSC).[62,63] It has been hypothesized that the internalized nanoparticles in cells could act as granules and scatter more lights, which could be collected using flow cytometry. Therefore, we performed flow cytometric analysis to assess the internalization of AgNPs in both bacteria strains and cancer cell lines.

Figures 8 and 9 display the density plots of flow cytometry light scattering before and after treating both bacteria and cancer cell lines with 5.0 and 20.0 $\mu g{\cdot}mL^{-1}$ AgNPs for the indicated times. The SSC intensity for both pathogens after treatment with 5.0 and 20.0 $\mu g{\cdot}mL^{-1}$ AgNPs slightly increased in compared with that of the control cells, indicating the internalization of synthesized AgNPs. It is interesting that *E. coli* displays a higher scattering in comparison to *S. aureus*, meaning more uptake of the biosynthesized AgNPs. The difference may be due to the distinct adherence to the charged bacterial cell wall or the affinity for phosphorus- and sulfur-containing compounds on the cell within a certain processing time. Moreover, the SSC values obtained after treatment with 5.0 $\mu g{\cdot}mL^{-1}$ AgNPs for both pathogens are slightly higher than those obtained after treatment with 20.0 $\mu g{\cdot}mL^{-1}$ AgNPs. We

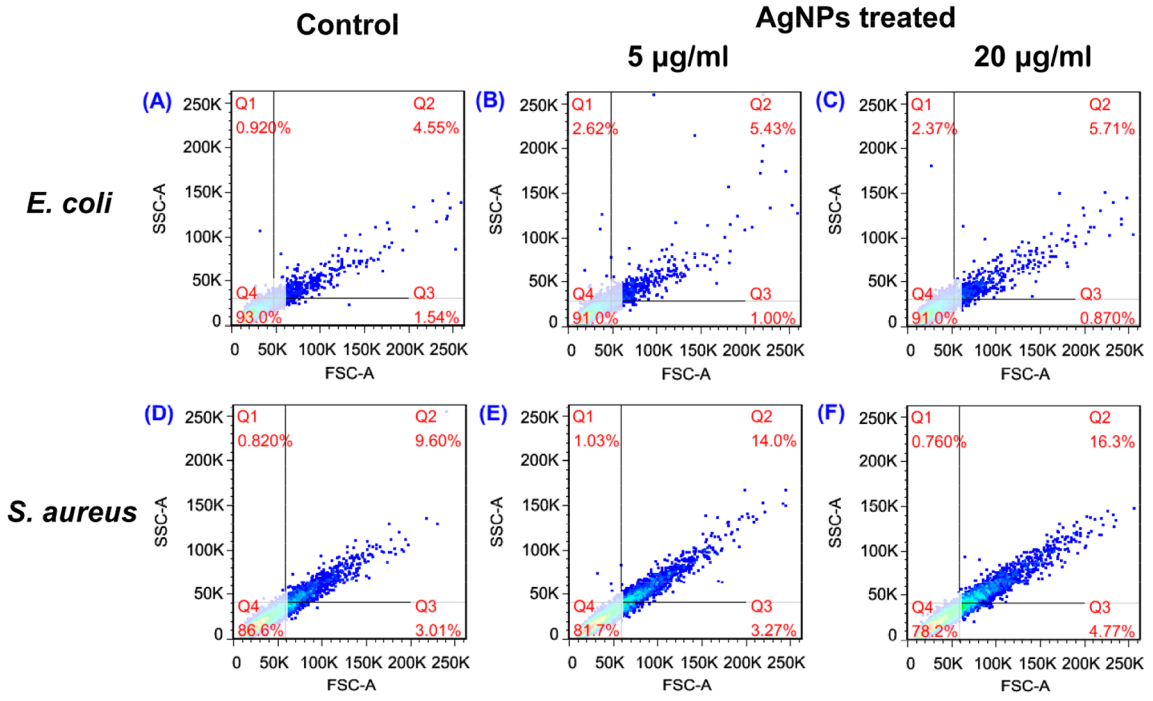

Figure 8. Uptake analysis of AgNPs with concentrations of (A) 0, (B) 5, and (C) 20 $\mu g{\cdot}ml^{-1}$ into *E. coli* and (D) 0, (E) 5, and (F) 20 $\mu g{\cdot}ml^{-1}$ into *S. aureus* as assessed by flow cytometry.

https://doi.org/10.1021/acsomega.1c06267
ACS Omega 2022, 7, 1494−1504

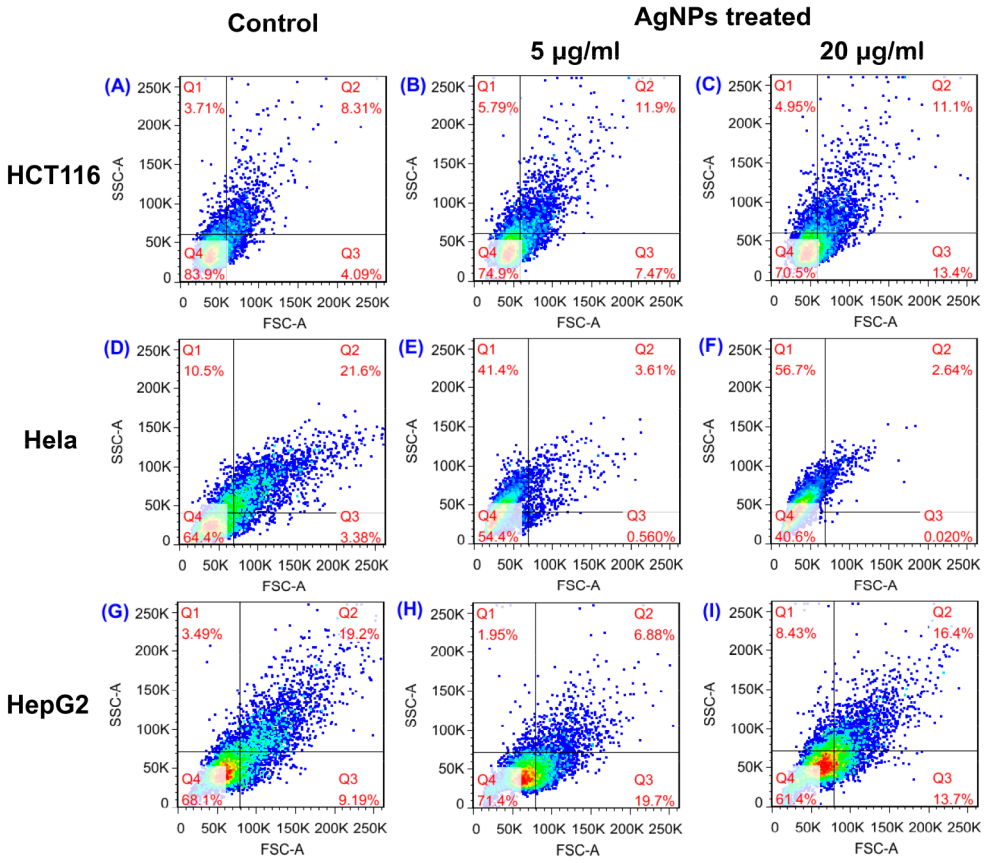

Figure 9. Uptake analysis of AgNPs with concentrations of (A) 0, (B) 5, and (C) 20 $\mu g \cdot ml^{-1}$ into HCT116; (D) 0, (E) 5, and (F) 20 $\mu g \cdot ml^{-1}$ into HepG2; and (G) 0, (H) 5, and (I) 20 $\mu g \cdot ml^{-1}$ into Hela cell lines as assessed by flow cytometry

speculated that after treatment with a high concentration of AgNPs, the cell wall and membrane were damaged and the granules could run off from the cytoplasm.[59] Combining these results with the MICs of AgNPs against both *E. coli* and *S. aureus*, it is possible that the cell wall and membrane of *S. aureus* are susceptible to the AgNPs biosynthesized by the *Mentha pulegium* leaf extract.

The uptake analysis of AgNPs into HCT116, HepG2, and HeLa cancer cell lines was also performed. The SSC values for HCT116 and HeLa cancer cell lines show a significance increase at both concentrations, indicating AgNP internalization. However, for the HepG2 cancer cell line the SSC value decreases from 3.45% to 1.95% after treatment with 5.0 $\mu g \cdot mL^{-1}$ AgNPs, which may result from the leakage of granules into the cytoplasm. This result indicates that AgNPs biosynthesized by *Mentha pulegium* leaf extract may cause necrosis by disintegrating the cell wall and membrane, which is assumed to be primary mechanism of cell death. Briefly, nanoparticle adhesion to the cell membrane would trigger cell morphological changes and thus result in the disruption of membrane permeability and respiratory functions via membrane depolarization. The increased membrane permeability and disruption of the cell wall would lead to the leak of cellular content, including proteins, enzymes, DNA, ions, metabolites, and the energy reservoir, into environment. The disintegrated cell wall and membrane would facilitate the uptake of AgNPs into the cell, which has been confirmed by the flow cytometry analysis at 20.0 $\mu g \cdot mL^{-1}$ AgNPs (SSC = 8.43%). Otherwise, we found that after treatment with a high concentration of AgNPs, the changes of the SSC intensity revealed different trends, where the SSC values for HCT116 decreased to 4.95% and those for Hela increased to 56.7%. The slightly decreased SSC value for HCT116 may due to the leak of cellular content, and the increased value indicates the more uptake of AgNPs. It seems that the mechanism of cell death originating from AgNPs in different cell lines is variant. For HCT116 and HepG2 cell lines, both cell wall damage and intracellular damage may be responsible for the cell death. However, for Hela cell line the cell death may be rooted in the formation of ROS or intracellular penetration. To disclose the precise mechanism of cell death, more sophisticated experiments should be performed.

3. CONCLUSION

In this study, the bioactive silver nanoparticles (AgNPs) were successfully fabricated using *Mentha pulegium* leaf extract under alkaline conditions with ultrasonic radiation at ambient temperature. The effects of biosynthesis parameters on the formation, average size, and polydispersity of AgNPs were also assessed. Characterization of as-prepared AgNPs revealed that the crystalline structure, average size, and surface loadings were entirely different from those synthesized by *Mentha pulegium* under acidic conditions. Furthermore, as-prepared materials were applied for biological activities like antioxidant, antibacterial, and anticancer activities. The results displayed that the anticancer activities were enhanced significantly. The flow cytometric analysis for both pathogens and cancer cell strains displayed a significant change in the SSC value with a variant trend, indicating the different mechanisms of cell death.

https://doi.org/10.1021/acsomega.1c06267
ACS Omega 2022, 7, 1494−1504

These results confirmed that the as-prepared AgNPs could be also useful for the development of new alternative biological agents in biomedicine, especially for anticancer efficacy.

4. EXPERIMENTAL SECTION

4.1. Chemicals. *Mentha pulegium* was purchased from a local pharmaceutical factory (Shaanxi Sciendan Pharmaceutical Co., Ltd., Xi'an, China). Other reagents, such as silver nitrate ($AgNO_3$, 99.8%), sodium chloride, yeast powder, 1,1-diphenyl-2-picrylhydrazulin (DPPH, > 99.5%), 3-(4,5-dimethyl-2-thiazolyl)-2,5-diphenyl-2*H*-tetrazolium bromine (MTT), dimethyl sulfoxide (DMSO), and so on, were bought as described in our previous studies.[30] The purity of all chemicals was analytical grade, which was not enhanced further. Ultrapure Milli-Q water was used to prepare all solutions.

4.2. Synthesis of Silver Nanoparticles. In this study, an easy and eco-friendly method for the green fabrication of bioactive AgNPs was developed using the leaf extract of *Mentha pulegium* under ultrasonic radiation at ambient temperature. The specific processes are as follows. The *Mentha pulegium* leaves (5.0 g) were ground to powder and then added into 100 mL of deionized water with ultrasonic radiation for 4.0 h. After filtration, the extract of the *Mentha pulegium* leaf was obtained, which was stored in 4 °C for further studies. Then, 5.0 mL of the aqueous extract was combined with 5.0 mL of 10 mM $AgNO_3$ to biosynthesize AgNPs under ultrasonic radiation. After 30 min of centrifugation at 10 000 rpm, the pure AgNPs could be obtained from the mixture. The resulting precipitates were washed several times using deionized water and then lyophilized for 12.0 h. The pH of the *Mentha pulegium* extract was adjusted with a certain concentration of NaOH to desired values. After adding $AgNO_3$ for the reduction reaction, the pH value of the mixture did not have any obvious change, which was monitored and determined by a pH meter.

4.3. Characterization of Silver Nanoparticles. To monitor the formation of AgNPs, the spectrum of the mixture ranging from 200 to 800 nm was periodically collected by using a UV−vis spectrophotometer (UV-2600, Japan). Transmission electron microscopy (TEM) was performed with a JEM-2100 Plus microscope equipped with an energy dispersive X-ray spectroscopy (EDX) attachment. Both were used to characterize the morphology of the AgNPs, whose crystalline nature was confirmed by HRTEM and selected area electron diffraction (SAED). The polydispersity and surface loads of the AgNPs were evaluated by measuring the polydispersity index and ζ-potential using a Malvern Zetasizer Nanoseries (ZEN 3600, Malvern, UK) instrument.

4.4. Antioxidant Activity of Silver Nanoparticles. To assess the antioxidant activity, serial concentrations of AgNPs (1.0 mL) were added to 1.0 mL of a 1,1-diphenyl-2-picrylhydrazulin solution (DPPH, 2.5 $\mu g \cdot mL^{-1}$), which was vigorously shaken and incubated for 30 min in the dark at room temperature. The absorbance of DPPH at 517 nm in ethanol would be quenched to some extent due to the addition of antioxidative AgNPs. The absorption of the negative control group (without AgNPs) was subtracted from each group of reaction mixture. The DPPH scavenging rate could be obtained by the following equation:

$$\text{Scavenging rate}\ (\%) = [1 - (A_1 - A_2)/A_0] \times 100\%$$

where A_0 is the absorbance of the DPPH and ultrapure water at 517 nm, A_1 is the absorbance of DPPH and AgNPs at 517 nm, and A_2 is the absorbance of ethanol and AgNPs at 517 nm.

4.5. Antibacterial Activity of Silver Nanoparticles. The growth inhibition studies of AgNPs against both *S. aureus* and *E. coli* were conducted in Luria−Bertani (LB) broth media. The experiments were carried out as per our previous illustration.[30] Briefly, 50 μL of the freshly prepared bacterial suspensions was added into 96-well plates, which contain desired amount of AgNPs and 50 μL of LB broth media in each hole. The plates were then incubated in a rotary shaker at 160 rpm at 37 °C. The increase of bacterial absorption at 600 nm was monitored every hour for 24.0 h. The control experiments, which contained only media and bacteria devoid of AgNPs, were also performed for both pathogens.

4.6. Anticancer Activity of Silver Nanoparticles. The well-cultured human colorectal cancer HCT116, hepatoma cancer HepG2, and cervical cancer (HeLa) cell lines were plated out in flat-bottom 96-well plates at a density of 1×10^4 cells per well and allowed to attach for 24.0 h. After removing the supernatant, the desired amount of AgNPs (0.8−100.0 $\mu g \cdot mL^{-1}$) was added into 96-well plates, which were cultured at 37 °C in an atmosphere of 5% CO_2 for 24.0 h. Then, 20 mL of thiazolyl blue tetrazolium bromide (MTT, 5.0 $\mu g \cdot mL^{-1}$) and 150 mL of DMEM medium were injected into each well. After 4.0 h of incubation, the media were gently removed to collect the formed formazan crystals, which were dissolved in 150 μL of DMSO before their absorbance was measured at 490 nm. The cell viability could be obtained by complying with the following formula:

$$\text{Cell viability}\ (\%) = (A - A_b)/(A_0 - A_b) \times 100\%$$

where A is the absorbance of the sample, A_b is the bleaching absorbance without the sample, and A_0 is the absorbance value of the control.

4.7. Internalization of Silver Nanoparticles. According to a previous study,[63] light scattering principles could be utilized to assess the internalization of nanoparticles in both bacteria and cancer cell lines. Thus, flow cytometric analysis was performed. All the cells referred to in the study were seeded in 6-well culture plates and combined with 5.0 and 20.0 $\mu g \cdot mL^{-1}$ AgNPs for 12.0 h of incubation. After this, these cells were harvested and resuspended for the flow cytometric experiments, where light scattering signals were collected and detected with corresponding detection channels after excitation with 488 nm lasers. The FlowJo 7.6.1 software was utilized to analyze the output data.

■ ASSOCIATED CONTENT

Supporting Information

The Supporting Information is available free of charge at https://pubs.acs.org/doi/10.1021/acsomega.1c06267.

Pictures of the mixed solution at different pH levels and the tests of zone inhibition and average size, polydispersity index, and ζ-potential of AgNPs synthesized with different biosynthesis parameters (PDF)

■ AUTHOR INFORMATION

Corresponding Author

Simin Wei − *State Key Laboratory of Research & Development of Characteristic Qin Medicine Resources (Cultivation), Co-Construction Collaborative Innovation*

https://doi.org/10.1021/acsomega.1c06267
ACS Omega 2022, 7, 1494−1504

Center for Chinese Medicine Resources Industrialization by Shaanxi and Education Ministry, Shaanxi University of Chinese Medicine, Xianyang 712083, China; orcid.org/0000-0001-9818-7595; Email: weisimin@iccas.ac.cn

Author

Yinghui Wang − *College of Science, Chang'an University, Xi'an 710064, China;* orcid.org/0000-0001-7617-7433

Complete contact information is available at: https://pubs.acs.org/10.1021/acsomega.1c06267

Notes

The authors declare no competing financial interest.

■ ACKNOWLEDGMENTS

This work was financially supported by the National Natural Science Foundation of China (Grant 22103007); the Key Scientific Research Plan of Shaanxi Provincial Department of Education (Grant 21JY009); the Natural Science Foundation of Shaanxi Province (Grant 2021JQ-221); the Young Talent fund of University Association for Science and Technology in Shaanxi, China (Grant 20190307), and the Fundamental Research Funds for the Central Universities, CHD (Grant 300102120303).

■ REFERENCES

(1) Kang, H.; Buchman, J. T.; Rodriguez, R. S.; Ring, H. L.; He, J.; Bantz, K. C.; Haynes, C. L. Stabilization of Silver and Gold Nanoparticles: Preservation and Improvement of Plasmonic Functionalities. *Chem. Rev.* **2019**, *119* (1), 664−699.

(2) Chen, Y.; Fan, Z. X.; Zhang, Z. C.; Niu, W. X.; Li, C. L.; Yang, N. L.; Chen, B.; Zhang, H. Two-Dimensional Metal Nanomaterials: Synthesis, Properties, and Applications. *Chem. Rev.* **2018**, *118* (13), 6409−6455.

(3) Choudhury, H.; Pandey, M.; Lim, Y. Q.; Low, C. Y.; Lee, C. T.; Marilyn, T. C. L.; Loh, H. S.; Lim, Y. P.; Lee, C. F.; Bhattamishra, S. K.; Kesharwani, P.; Gorain, B. Silver nanoparticles: Advanced and promising technology in diabetic wound therapy. *Mater. Sci. Eng. C-Mater. Biol. Appl.* **2020**, *112*, 110925.

(4) Jouyban, A.; Rahimpour, E. Optical sensors based on silver nanoparticles for determination of pharmaceuticals: An overview of advances in the last decade. *Talanta* **2020**, *217*, 121071.

(5) Nene, A.; Galluzzi, M.; Hongrong, L.; Somani, P.; Ramakrishna, S.; Yu, X. F. Synthetic preparations and atomic scale engineering of silver nanoparticles for biomedical applications. *Nanoscale* **2021**, *13* (33), 13923−13942.

(6) Abbas, M.; Atiq, A.; Xing, R. R.; Yan, X. H. Silver-incorporating peptide and protein supramolecular nanomaterials for biomedical applications. *J. Mater. Chem. B* **2021**, *9* (22), 4444−4458.

(7) Bruna, T.; Maldonado-Bravo, F.; Jara, P.; Caro, N. Silver Nanoparticles and Their Antibacterial Applications. *Int. J. Mol. Sci.* **2021**, *22* (13), 7202.

(8) Oves, M.; Ahmar Rauf, M.; Aslam, M.; Qari, H. A.; Sonbol, H.; Ahmad, I.; Sarwar Zaman, G.; Saeed, M. Green synthesis of silver nanoparticles by Conocarpus Lancifolius plant extract and their antimicrobial and anticancer activities. *Saudi J. Biol. Sci.* **2021**, 460−471, DOI: 10.1016/j.sjbs.2021.09.007.

(9) Oves, M.; Aslam, M.; Rauf, M. A.; Qayyum, S.; Qari, H. A.; Khan, M. S.; Alam, M. Z.; Tabrez, S.; Pugazhendhi, A.; Ismail, I. M. I. Antimicrobial and anticancer activities of silver nanoparticles synthesized from the root hair extract of Phoenix dactylifera. *Mater. Sci. Eng. C-Mater. Biol. Appl.* **2018**, *89*, 429−443.

(10) Nikaeen, G.; Abbaszadeh, S.; Yousefinejad, S. Application of nanomaterials in treatment, anti-infection and detection of coronaviruses. *Nanomedicine* **2020**, *15* (15), 1501−1512.

(11) Dasari, S.; Yedjou, C. G.; Brodell, R. T.; Cruse, A. R.; Tchounwou, P. B. Therapeutic strategies and potential implications of silver nanoparticles in the management of skin cancer. *Nanotechnol. Rev.* **2020**, *9* (1), 1500−1521.

(12) Yan, N.; Tang, B. Z.; Wang, W.-X. In Vivo Bioimaging of Silver Nanoparticle Dissolution in the Gut Environment of Zooplankton. *ACS Nano* **2018**, *12* (12), 12212−12223.

(13) Prasher, P.; Sharma, M.; Mudila, H.; Gupta, G.; Sharma, A. K.; Kumar, D.; Bakshi, H. A.; Negi, P.; Kapoor, D. N.; Chellappan, D. K.; Tambuwala, M. M.; Dua, K. Emerging trends in clinical implications of bio-conjugated silver nanoparticles in drug delivery. *Colloid Interface Sci.* **2020**, *35*, 100244.

(14) Oves, M.; Khan, M. S.; Zaidi, A.; Ahmed, A. S.; Ahmed, F.; Ahmad, E.; Sherwani, A.; Owais, M.; Azam, A. Antibacterial and Cytotoxic Efficacy of Extracellular Silver Nanoparticles Biofabricated from Chromium Reducing Novel OS4 Strain of Stenotrophomonas maltophilia. *PLoS One* **2013**, *8* (3), e59140.

(15) Banu, A. N.; Kudesia, N.; Raut, A. M.; Pakrudheen, I.; Wahengbam, J. Toxicity, bioaccumulation, and transformation of silver nanoparticles in aqua biota: A review. *Environ. Chem. Lett.* **2021**, *19*, 4275.

(16) Nesovic, K.; Miskovic-Stankovic, V. A comprehensive review of the polymer-based hydrogels with electrochemically synthesized silver nanoparticles for wound dressing applications. *Polym. Eng. Sci.* **2020**, *60* (7), 1393−1419.

(17) Tortella, G. R.; Rubilar, O.; Duran, N.; Diez, M. C.; Martinez, M.; Parada, J.; Seabra, A. B. Silver nanoparticles: Toxicity in model organisms as an overview of its hazard for human health and the environment. *J. Hazard. Mater.* **2020**, *390*, 121974.

(18) Slepicka, P.; Kasalkova, N. S.; Siegel, J.; Kolska, Z.; Svorcik, V. Methods of Gold and Silver Nanoparticles Preparation. *Materials* **2020**, *13* (1), 1.

(19) Jara, N.; Milan, N. S.; Rahman, A.; Mouheb, L.; Boffito, D. C.; Jeffryes, C.; Dahoumane, S. A. Photochemical Synthesis of Gold and Silver Nanoparticles-A Review. *Molecules* **2021**, *26* (15), 4585.

(20) Cubova, K.; Cuba, V. Synthesis of inorganic nanoparticles by ionizing radiation - a review. *Radiat. Phys. Chem.* **2020**, *169*, 108774.

(21) Iriarte-Mesa, C.; Lopez, Y. C.; Matos-Peralta, Y.; de la Vega-Hernandez, K.; Antuch, M. Gold, Silver and Iron Oxide Nanoparticles: Synthesis and Bionanoconjugation Strategies Aimed at Electrochemical Applications. *Top. Curr. Chem.* **2020**, *378* (1), 12.

(22) Tarannum, N.; Divya; Gautam, Y. K. Facile green synthesis and applications of silver nanoparticles: A state-of-the-art review. *RSC Adv.* **2019**, *9* (60), 34926−34948.

(23) Beyene, H. D.; Werkneh, A. A.; Bezabh, H. K.; Ambaye, T. G. Synthesis paradigm and applications of silver nanoparticles (AgNPs), a review. *Sustainable Mater. Technol.* **2017**, *13*, 18−23.

(24) Vanlalveni, C.; Lallianrawna, S.; Biswas, A.; Selvaraj, M.; Changmai, B.; Rokhum, S. L. Green synthesis of silver nanoparticles using plant extracts and their antimicrobial activities: a review of recent literature. *RSC Adv.* **2021**, *11* (5), 2804−2837.

(25) Tehri, N.; Vashishth, A.; Gahlaut, A.; Hooda, V. Biosynthesis, antimicrobial spectra and applications of silver nanoparticles: Current progress and future prospects. *Inorg. Nano-Met. Chem.* **2020**, 1.

(26) Jadhav, K.; Deore, S.; Dhamecha, D.; H R, R.; Jagwani, S.; Jalalpure, S.; Bohara, R. Phytosynthesis of Silver Nanoparticles: Characterization, Biocompatibility Studies, and Anticancer Activity. *ACS Biomater. Sci. Eng.* **2018**, *4* (3), 892−899.

(27) Roy, A.; Bulut, O.; Some, S.; Mandal, A. K.; Yilmaz, M. D. Green synthesis of silver nanoparticles: biomolecule-nanoparticle organizations targeting antimicrobial activity. *RSC Adv.* **2019**, *9* (5), 2673−2702.

(28) Alsammarraie, F. K.; Wang, W.; Zhou, P.; Mustapha, A.; Lin, M. Green synthesis of silver nanoparticles using turmeric extracts and investigation of their antibacterial activities. *Colloid. Surface B* **2018**, *171*, 398−405.

(29) Bagherzade, G.; Tavakoli, M. M.; Namaei, M. H. Green synthesis of silver nanoparticles using aqueous extract of saffron

(Crocus sativus L.) wastages and its antibacterial activity against six bacteria. *Asian Pac. J. Trop. Bio.* **2017**, *7* (3), 227−233.
(30) Wei, S. M.; Wang, Y. H.; Tang, Z. S.; Hu, J. H.; Su, R.; Lin, J. J.; Zhou, T.; Guo, H.; Wang, N.; Xu, R. R. A size-controlled green synthesis of silver nanoparticles by using the berry extract of *Sea Buckthorn* and their biological activities. *New J. Chem.* **2020**, *44* (22), 9304−9312.
(31) Wang, Y.; Wei, S.; Wang, K.; Wang, Z.; Duan, J.; Cui, L.; Zheng, H.; Wang, Y.; Wang, S. Evaluation of biosynthesis parameters, stability and biological activities of silver nanoparticles synthesized by *Cornus Officinalis* extract under 365 nm UV radiation. *RSC Adv.* **2020**, *10* (45), 27173−27182.
(32) He, Y. Q.; Wei, F. F.; Ma, Z. Y.; Zhang, H.; Yang, Q.; Yao, B. H.; Huang, Z. R.; Li, J.; Zeng, C.; Zhang, Q. Green synthesis of silver nanoparticles using seed extract of Alpinia katsumadai, and their antioxidant, cytotoxicity, and antibacterial activities. *RSC Adv.* **2017**, *7* (63), 39842−39851.
(33) He, Y.; Li, X.; Wang, J.; Yang, Q.; Yao, B.; Zhao, Y.; Zhao, A.; Sun, W.; Zhang, Q. Synthesis, characterization and evaluation cytotoxic activity of silver nanoparticles synthesized by Chinese herbal *Cornus officinalis* via environment friendly approach. *Environ. Toxicol. Phar.* **2017**, *56*, 56−60.
(34) He, Y.; Li, X.; Zheng, Y.; Wang, Z.; Ma, Z.; Yang, Q.; Yao, B.; Zhao, Y.; Zhang, H. A green approach for synthesizing silver nanoparticles, and their antibacterial and cytotoxic activities. *New J. Chem.* **2018**, *42* (4), 2882−2888.
(35) Gondil, V. S.; Kalaiyarasan, T.; Bharti, V. K.; Chhibber, S. Antibiofilm potential of *Sea buckthorn* silver nanoparticles (SBT@AgNPs) against Pseudomonas aeruginosa. *3 Biotech* **2019**, *9* (11), 402.
(36) Wei, S.; Wang, Y.; Tang, Z.; Su, R.; Xu, H.; Chen, L.; Liu, S.; Li, C. Green synthesis of silver nanoparticles using *jujube* aqueous extract and evaluation of their antioxidant and antibacterial effects. *Nat. Prod. Res. Dev.* **2020**, *32* (2), 182−190.
(37) Sreekanth, T. V. M.; Ravikumar, S.; Eom, I. Y. Green synthesized silver nanoparticles using *Nelumbo nucifera* root extract for efficient protein binding, antioxidant and cytotoxicity activities. *J. Photochem. Photobiol., B* **2014**, *141*, 100−105.
(38) Premanand, G.; Shanmugam, N.; Kannadasan, N.; Sathishkumar, K.; Viruthagiri, G. *Nelumbo nucifera* leaf extract mediated synthesis of silver nanoparticles and their antimicrobial properties against some human pathogens. *Appl. Nanosci.* **2016**, *6* (3), 409−415.
(39) Wei, S.; Tang, Z.; Li, H.; Zhang, K.; Song, Z. Synthesis and antibacterial activity of silver nanoparticles synthesized by *Cornus officinalis* aqueous extract. *Chin. Tradit. Herb. Drugs* **2019**, *50* (1), 52−58.
(40) Wei, S.; Wang, Y.; Tang, Z.; Su, R.; Hu, J.; Guo, H.; Li, C.; Jiang, J.; Song, Z. Novel Biosynthesis Method of Silver Nanoparticle by UV Radiation of *Cornus Officinalis* Aqueous Extract and Biological Activities. *Chem. J. Chin. Univ.-Chin.* **2020**, *41* (6), 1391−1398.
(41) El Hassani, F. Z. Characterization, activities, and ethnobotanical uses of *Mentha* species in Morocco. *Heliyon* **2020**, *6* (11), No. e05480.
(42) Politeo, O.; Bektasevic, M.; Carev, I.; Jurin, M.; Roje, M. Phytochemical Composition, Antioxidant Potential and Cholinesterase Inhibition Potential of Extracts from *Mentha pulegium* L. *Chem. Biodivers.* **2018**, *15* (12), No. e1800374.
(43) Benabdallah, A.; Rahmoune, C.; Boumendjel, M.; Aissi, O.; Messaoud, C. Total phenolic content and antioxidant activity of six wild *Mentha* species (Lamiaceae) from northeast of Algeria. *Asian Pac. J. Trop. Bio.* **2016**, *6* (9), 760−766.
(44) Hassanpour, H.; Khavari-Nejad, R. A.; Niknam, V.; Razavi, K.; Najafi, F. Effect of penconazole and drought stress on the essential oil composition and gene expression of *Mentha pulegium* L. (Lamiaceae) at flowering stage. *Acta Physiol. Plant.* **2014**, *36* (5), 1167−1175.
(45) Abd Kelkawi, A. H.; Kajani, A. A.; Bordbar, A. K. Green synthesis of silver nanoparticles using Mentha pulegium and investigation of their antibacterial, antifungal and anticancer activity. *Iet Nanobiotechnol.* **2017**, *11* (4), 370−376.
(46) Gholami, M.; Azarbani, F.; Hadi, F. Silver nanoparticles synthesised by using Iranian *Mentha pulegium* leaf extract as a non-cytotoxic antibacterial agent. *Mater. Technol.* **2021**, 1−9.
(47) Liu, H.; Zhang, H.; Wang, J.; Wei, J. Effect of temperature on the size of biosynthesized silver nanoparticle: Deep insight into microscopic kinetics analysis. *Arab. J. Chem.* **2020**, *13* (1), 1011−1019.
(48) Kaur, G.; Kalia, A.; Sodhi, H. S. Size controlled, time-efficient biosynthesis of silver nanoparticles from Pleurotus florida using ultra-violet, visible range, and microwave radiations. *Inorg. Nano-Met. Chem.* **2020**, *50* (1), 35−41.
(49) Laid, T. M.; Abdelhamid, K.; Eddine, L. S.; Abderrhmane, B. Optimizing the biosynthesis parameters of iron oxide nanoparticles using central composite design. *J. Mol. Struct.* **2021**, *1229*, 129497.
(50) Wei, S. M.; Wang, Y. H.; Tang, Z. S.; Xu, H. B.; Wang, Z.; Yang, T.; Zou, T. Y. A novel green synthesis of silver nanoparticles by the residues of Chinese herbal medicine and their biological activities. *RSC Adv.* **2021**, *11* (3), 1411−1419.
(51) Wei, S.; Wang, Y.; Tang, Z.; Wang, Z.; Zhang, Z.; Su, R.; Jin, R.; Song, Z. Preparation of silver nanoparticles by extract of Yinqiao Jiedu Mixture waste and its antioxidative and antibacterial activity evaluation. *Chin. Tradit. Herb. Drugs* **2020**, *51* (16), 4169−4175.
(52) Khan, S.; Singh, S.; Gaikwad, S.; Nawani, N.; Junnarkar, M.; Pawar, S. V. Optimization of process parameters for the synthesis of silver nanoparticles from Piper betle leaf aqueous extract, and evaluation of their antiphytofungal activity. *Environ. Sci. Pollut. Res. Int.* **2020**, *27* (22), 27221−27233.
(53) Sathishkumar, M.; Sneha, K.; Won, S. W.; Cho, C. W.; Kim, S.; Yun, Y. S. Cinnamon zeylanicum bark extract and powder mediated green synthesis of nano-crystalline silver particles and its bactericidal activity. *Colloid Surf. B* **2009**, *73* (2), 332−338.
(54) Heydari, R.; Rashidipour, M. Green synthesis of silver nanoparticles using extract of oak fruit hull (jaft): Synthesis and in vitro cytotoxic effect on mcf-7 cells. *Int. J. Breast Cancer* **2015**, *2015*, 846743.
(55) Manosalva, N.; Tortella, G.; Diez, M. C.; Schalchli, H.; Seabra, A. B.; Duran, N.; Rubilar, O. Green synthesis of silver nanoparticles: Effect of synthesis reaction parameters on antimicrobial activity. *World J. Microbiol. Biotechnol.* **2019**, *35* (6), 88.
(56) Chaudhary, V.; Chavali, M. Novel methyl-orange assisted core-shell polyaniline-silver nanosheets for highly sensitive ammonia chemiresistors. *J. Appl. Polym. Sci.* **2021**, *138* (43), No. 51288.
(57) KÜP, F. O.; Coskuncay, S.; Duman, F. Biosynthesis of silver nanoparticles using leaf extract of Aesculus hippocastanum (horse chestnut): Evaluation of their antibacterial, antioxidant and drug release system activities. *Mater. Sci. Eng., C* **2020**, *107*, 110207.
(58) Fafal, T.; Tastan, P.; Tuzun, B. S.; Ozyazici, M.; Kivcak, B. Synthesis, characterization and studies on antioxidant activity of silver nanoparticles using Asphodelus aestivus Brot. aerial part extract. *S. Afr. J. Bot.* **2017**, *112*, 346−353.
(59) Kumari, M.; Shukla, S.; Pandey, S.; Giri, V. P.; Bhatia, A.; Tripathi, T.; Kakkar, P.; Nautiyal, C. S.; Mishra, A. Enhanced Cellular Internalization: A Bactericidal Mechanism More Relative to Biogenic Nanoparticles than Chemical Counterparts. *ACS Appl. Mater. Interfaces* **2017**, *9* (5), 4519−4533.
(60) Dipankar, C.; Murugan, S. The green synthesis, characterization and evaluation of the biological activities of silver nanoparticles synthesized from Iresine herbstii leaf aqueous extracts. *Colloid Surf. B* **2012**, *98*, 112−119.
(61) Xu, L.; Wang, Y. Y.; Huang, J.; Chen, C. Y.; Wang, Z. X.; Xie, H. Silver nanoparticles: Synthesis, medical applications and biosafety. *Theranostics* **2020**, *10* (20), 8996−9031.
(62) Wu, Y.; Ali, M. R. K.; Dansby, K.; El-Sayed, M. A. Improving the Flow Cytometry-based Detection of the Cellular Uptake of Gold Nanoparticles. *Anal. Chem.* **2019**, *91* (22), 14261−14267.
(63) Suzuki, H.; Toyooka, T.; Ibuki, Y. Simple and Easy Method to Evaluate Uptake Potential of Nanoparticles in Mammalian Cells

https://doi.org/10.1021/acsomega.1c06267
ACS Omega 2022, 7, 1494−1504

Using a Flow Cytometric Light Scatter Analysis. *Environ. Sci. Technol.* **2007**, *41* (8), 3018−3024.

https://doi.org/10.1021/acsomega.1c06267
ACS Omega 2022, 7, 1494−1504